Supplementary Material for Modeling the hydrological responses to changing climate and land use/land cover across contrasting agroecological environments: A case study in Chemoga watershed in the Upper Blue Nile Basin, Ethiopia

Taye Minichil Meshesha [1,2,*], Atsushi Tsunekawa [3], Nigussie Haregeweyn [4], Mitsuru Tsubo [3], Ayele Almaw Fenta [4], Mulatu Liyew Berihun [5,6], Arega Mulu [2], Ashebir Sewale Belay [7], Dagnenet Sultan [3,6], Kindiye Ebabu [8], Tadesual Asamin Setargie [6,9], Samuel Berihun Kassa [1,2], Yoseph Buta Hailu [1,2], Takashi Abe [4]

[1] The United Graduate School of Agricultural Sciences, Tottori University, 4-101 Koyama-Minami, Tottori 680-8553, Japan.

[2] School of Civil and Water Resource Engineering, Debre Markos Institute of Technology, Debre Markos University, P.O. Box 269, Debre Markos, Ethiopia.

[3] Arid Land Research Center, Tottori University, 1390 Hamasaka, Tottori 680-0001, Japan.

[4] International Platform for Dryland Research and Education, Tottori University, 1390 Hamasaka, Tottori 680-0001, Japan.

[5] Department of Agricultural and Biological Engineering, Tropical Research and Education Center, IFAS, University of Florida, Homestead, FL, USA.

[6] Faculty of Civil and Water Resources Engineering, Bahir Dar Institute of Technology, Bahir Dar University, P.O. Box 26, Bahir Dar, Ethiopia.

[7] School of Earth Sciences, Bahir Dar University, P.O. Box 79, Bahir Dar, Ethiopia.

[8] College of Agriculture and Environmental Sciences, Bahir Dar University, P.O. Box 5501, Bahir Dar, Ethiopia.

[9] Blue Nile Water Institute, Bahir Dar University, Bahir Dar, Ethiopia.

Corresponding author: Taye Minichil Meshesha (m.tayemeshesha21@gmail.com)

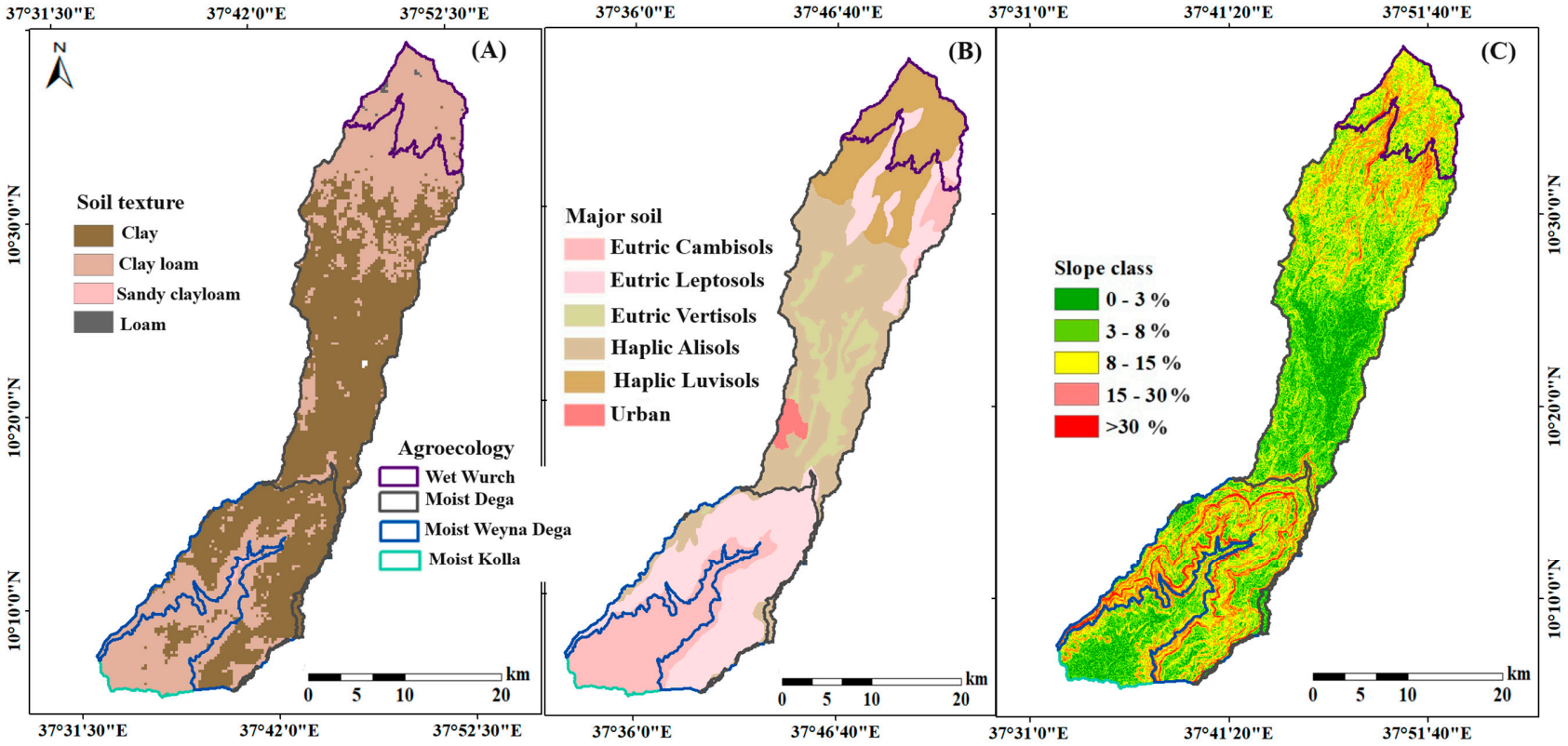

Figure S1. Major soil textures (A), types (B), and slope classes (C) within distinct agroecological regions in Chemoga watershed.

Table S1. Typical characteristics of four agroecological environments in Chemoga watershed.

	Typical characteristics			
	Wet Wurch	Moist Dega	Moist Weyna Dega	Moist Kolla
Mean annual temperature range (°C)	4.7–17.4	8.8–22.7	13.9–25.5	15.7–28.9
Mean annual rainfall (mm)	1513	1311	1251	1108
Altitude (m)	>3200	2300–3200	1500–2300	< 1500
Major crops	Barley and potato	Wheat, teff, barley, potato, fava bean and engido (*Avena* spp.)	Maize, wheat, and teff	Sorghum, maize, and haricot bean
Slope class (% range)	Area contribution to each slope classes (%)			
Flat (0–3)	0.8	7.9	2.0	21.2
Gentle (3–8)	6.7	27.3	12.0	42.5
Sloping (8–15)	26.8	29.6	23.3	19.0
Steep (15–30)	52.3	26.4	31.3	16.3
Very steep (>30)	13.5	8.8	31.5	1.0

Wet Wurch is characterized by steep slopes covering 52.3 % of its area. Moist Dega primarily consists of moderately sloping terrain, covering 29.6 % of its area. Around 31.5 % of the Moist Weyna Dega agroecology is covered by very steep slopes, whereas Moist Kolla is primarily covered by gentle slopes, covering 42.5 % of its area. The slope measurements were derived from SRTM–DEM data.

1A. Land use/land cover (LULC) change analysis

The LULC maps were produced from Landsat satellite images of TM, ETM+, and OLI for 1985, 1995, 2013, and 2020 with 30-m spatial resolution downloaded from the United States Geological Survey (https://earthexplorer.usgs.gov). In addition to Landsat satellite images, 12 aerial photographs (scale 1:50,000) taken in 1984 and 1985 obtained from the Ethiopian Mapping Agency (EMA) were used as auxiliary input data for the LULC classification of 1985. The images were selected by considering data availability, anticipated major LULC changes due to regime (Gov't) change and policies related to land use and agriculture by the government. Image was classified using hybrid (unsupervised and supervised) classification techniques [1]. Each Landsat image was iso-clustered into 500 classes. Supervised classification was then applied by geo-linking with Google Earth, and a pixel-based supervised classification to six LULC categories (built-up, cropland, forest, grassland, woodland, and water body). The analysis was done both at watershed scale and separately considering the four distinct agroecological environments within the watershed. Details can be found in [2].

The watershed level analysis evaluated changes from 1983 to 2020 and from 2021 to 2060. Cropland increased by 23 % in the earlier period and further increased by 3 % by 2060 under the business-as-usual (BAU). Woodland and grassland decreased by 23 % and 5 %, respectively, in the past 35 years and further decreased by 6 % and 3 %, respectively, by 2060 under the BAU LULC change scenario. In contrast, under the land conservation (LC) scenario, there was a significant shift towards forest restoration (8 % increase), along with the conservation of grasslands by 2060.

When considering the distinct agroecological environments, important transitions and changes were identified that were not apparent at the watershed level [2]. These transitions likely indicate more specific and localized alterations in LULC within these environments (Figure S2). In 1985, woodland dominated in Wet Wurch and Moist Kolla, while cropland dominated in Moist Dega and Moist Weyna Dega agroecological environments (Figure S2). Over the past 35 years, the most substantial changes in all agroecological environments were the expansion of cropland accompanied by the reduction of grassland in

Moist Dega and woodland in the other agroecological environments (Figure S2). The most substantial change was observed in Moist Kolla, where cropland increased dramatically by 53.5 %, followed by that in the Wet Wurch agroecology, where cropland increased by 27.1 % mainly at the expense of woodland during the historical study period. The projected BAU LULC change showed a further increase of cropland in the Moist Kolla agroecology by 28.1 % with the decline of woodland by 31.6 % expected in the future to 2060. In contrast, in the LC scenario there was a significant shift towards vegetation cover restoration over steep slopes, with a substantial increase in forest coverage (12.8 %) in the Moist Weyna Dega agroecology (Figure S2).

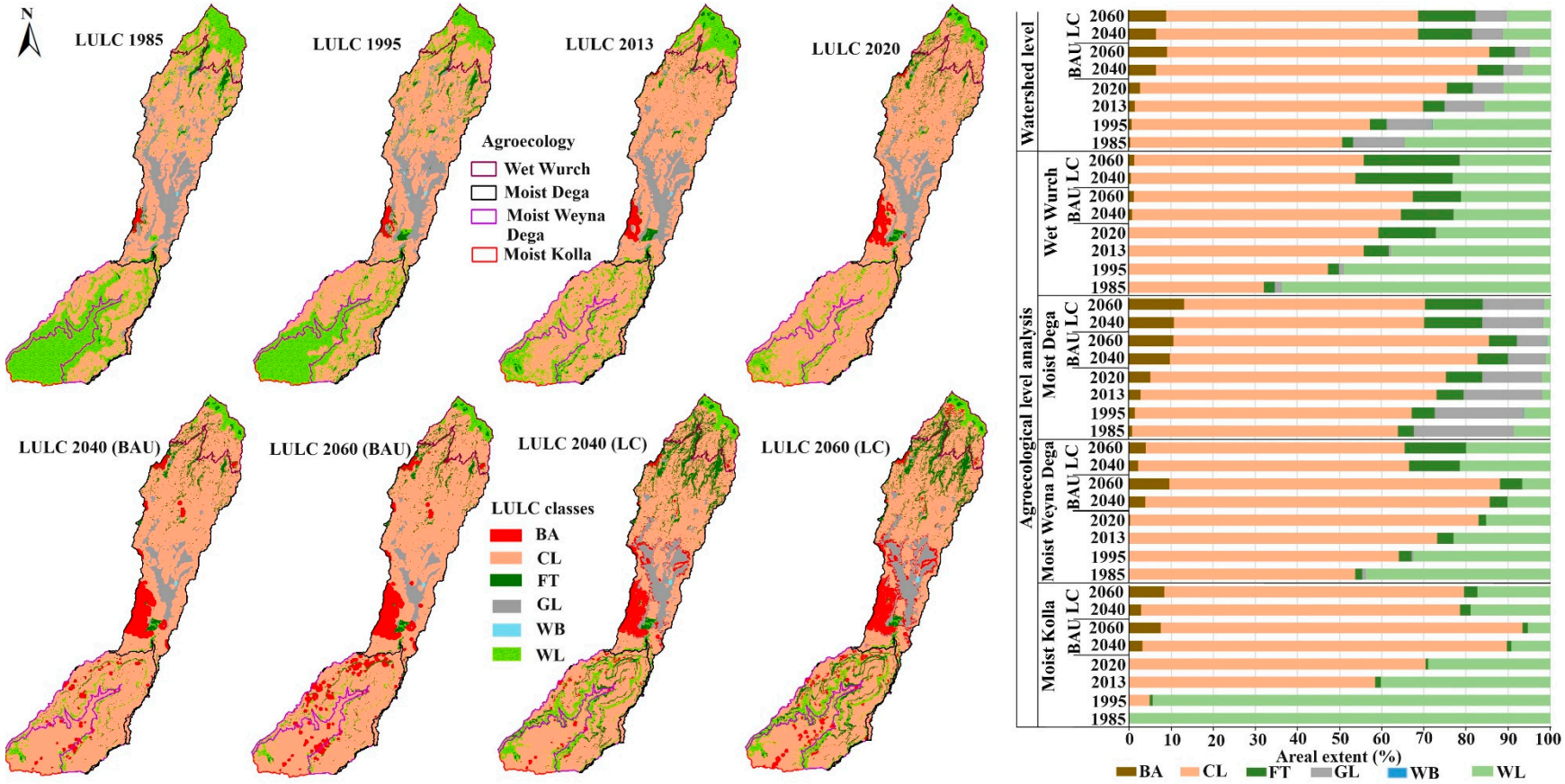

Figure S2. Land use land cover maps (left) and areal extent of land use and land cover (LULC) categories (right) at the watershed level and in four different agroecological environments. BAU and LC denotes for Projected LULC maps under business-as-usual and land conservation scenarios, respectively. BA: built-up area; CL: cropland; FT: Forest; GL: grassland; WB: water body; and WL: woodland (source:[2]).

1B. CA-Markov model

The hybrid CA-Markov model integrates CA as a spatial distribution of transitions with the Markov Chain probability matrix. Prediction of LULC changes using the CA-Markov model involves three main activities [3] (Figure S3): (1) the development of a probability matrix (Eq. 1) and an area matrix from a pair of past LULC maps using the Markov module, (2) creation of a suitability map that consists of factors and constraints, and (3) use of special allocation in the CA-Markov module (Eq. 2):

$$P = \begin{vmatrix} P_{11} & P_{12} & \cdots & P_{1n} \\ P_{21} & P_{22} & \cdots & P_{2n} \\ \cdots & \cdots & & \cdots \\ P_{n1} & P_{n2} & \cdots & P_{nm} \end{vmatrix} \quad (1)$$

where $\sum_{i=1}^{n} P_{ij} = 1, 0 \leq P_{ij}, P_{ij}$ is the transition probability from LULC type *i* to type *j*, and *n* is the number of LULC types.

$$L_{t+1} = P \times L_t \quad (2)$$

where L_t and L_{t+1} are the LULC at time of *t* and *t* + 1, respectively, and P is the transition probability matrix in a state that is calculated as follows:

The prediction capacity of the CA-Markov model was assessed by simulating the 2020 LULC map by using the 2005 and 2013 LULC maps and comparing with the simulated results to the classified 2020 LULC map. The simulated map of 2020 agreed very well with the classified LULC map of 2020, and the model validation results of K_{no} (96.3 %), $K_{location}$ (95.7 %), $K_{locationStrata}$ (95.7 %), and $K_{standard}$ (92.3 %). Finally, the validated hybrid CA-Markov model was used to produce the LULC maps of 2040 and 2060 under two alternative scenarios: business-as-usual and land conservation. Prediction of LULC changes using the CA-Markov model involves three main activities [3]: (1) the development of a probability matrix and an area matrix from a pair of past LULC maps using the Markov module, (2) creation of a suitability map that consists of factors and constraints using a multicriteria evaluation (MCE) module, and (3) use of special allocation in the CA-Markov model.

The suitability map is a combination of multiple factors and constraints used to guide the relative suitability of land allocation in the simulation of LULC change using the CA-Markov model [4]. Table S3 shows the factors and constraints considered for the LULC simulation.

Table S2. Factors and constraints considered and their weights for predicting LULC conditions in the Chemoga watershed.

LULC category	Factors	Factor weight	Consistency ratio	Constraints
Built-up	Suitable areas to built-up	0.6783	0.03	Slope > 15 %
	Distance to market centers	0.1388		Grassland
	Distance to road	0.1293		
	Slope	0.0537		
Cropland	Suitable areas to cropland	0.7854	0.07	Slope > 15 %
	Distance to rivers	0.0658		Grassland
	Slope	0.1488		
Forest	Suitable areas to forest	0.6716	0.07	
	Distance to rivers	0.0629		
	Slope	0.2654		
Grassland	Suitable areas to grassland	0.7695	0.03	
	Distance to river	0.1040		
	Slope	0.1265		
Water Body	Suitable areas to water body	0.4507	0.01	
	Distance to river	0.4901		
	Slope	0.0592		
Woodland	Suitable areas to woodland	0.6491	0.06	
	Slope	0.0719		
	Elevation	0.2790		

The suitability map for the BAU scenario was prepared from a weighted linear combination of factors for each LULC category (Table S2). The factors were standardized from 0 to 256 in a fuzzy membership function that implies 0 for less suitable and 256 for more suitable land for conversion to a specific LULC category. In the same way, the suitability map of the LC scenario was prepared by adding the constraints with Boolean images to the factors applied in the BAU scenario. The constraints were standardized to 0 (not suitable) or 1 (suitable) for land use conversion (Table S2, Figure S3).

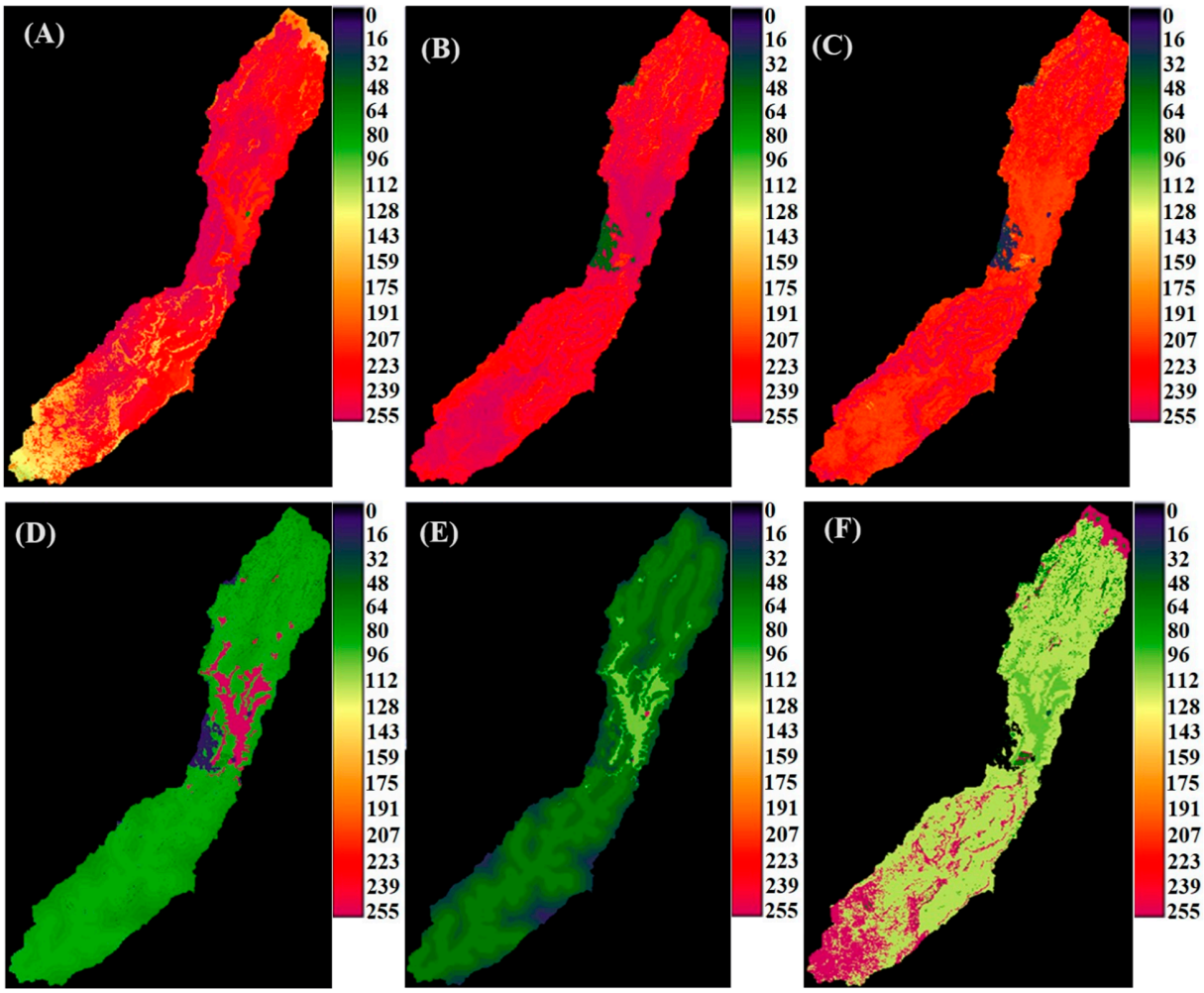

Figure S3. Suitability map for land allocation to (A) built-up, (B) cropland, (C) forest, (D) grassland, (E) water body, and (F) woodland in the Chemoga watershed.

The areal extent of losses, gains, and percentage of changes for each LULC change were computed using Eqs. (3), (4), and (5), respectively:

$$P_{loss(i),j} = \frac{(P_{i,j} - P_{j,i})}{(P_{ci} - P_{ri})} \times 100, i \neq j \quad (3)$$

$$P_{gain(i),j} = \frac{(P_{j,i} - P_{i,j})}{(P_{ci} - P_{ri})} \times 100, i \neq j \quad (4)$$

$$Percent\ change\ (\%) = \left(\frac{A_{i+1} - A_i}{A_1}\right) \times 100 \quad (5)$$

where $P_{loss\ (i),\ j}$ is the percentage taken by LULC category j from category i; $P_{gain(i),\ j}$ is the percentage taken by type i from category j; $P_{i,j}$ and $P_{j,i}$ are the individual entries in a given change matrix; P_{ci} is the column

total of type *i*; and P_{ri} is the row total for type *i*. A_1 is the area in year 1 and A_2 is the area in year 2 of a LULC type (ha).

The use of alternative scenarios to predict LULC is helpful for decision makers and local land use planners for effective and sustainable land management in the future [5,6]. The BAU and LC scenarios were formulated based on the land use and watershed characteristics of the study area and a literature review related to future land use plans [6] and land use policies of the Ethiopian government [2]. The BAU scenario assumed the continuation of recent past trends of socioeconomic activities related to LULC change without any management intervention, whereas the LC scenario was designed to consider management intervention for sustainable land use. The LC scenario considered the land capability approach, which avoids cultivation and settlement expansion on steep slopes (>15 %) [5,7], as well as the strict implementation of existing spatial policies of the Ethiopian government for forest and water body conservation [2].

2A. General Climate Models (GCMs)

From a thorough evaluation of over 31 available GCMs, ten were carefully selected for downscaling and ensemble use (Table S3), with the primary consideration being the availability of historical and future climate variables, such as precipitation and minimum and maximum temperatures, for both the SSP2-4.5 and SSP5-8.5 scenarios on a daily basis.

Table S3. Global climate models used in this study.

Model Name	Organization	Resolution (° lat. x long.)
ACCESS-CM2	Commonwealth Scientific and Industrial Research Organization, Australian Research Council Centre of Excellence for Climate System Science, Australia	1.250 x 1.875
INM-CM5-0	Institute for Numerical Mathematics, Russian Academy of Science, Moscow, Russia	1.500 x 2.000
CMCC-ESM2	Centro Euro-Mediterraneo sui Cambiamenti Climatici, Italy	0.938 x 1.250
CNRM-ESM2-1	National Center of Meteorological Research, France	1.406 x 1.406
EC-Earth3-Veg-LR	EC-Earth consortium, Rossby Center, Swedish Meteorological and Hydrological Institute, Sweden	1.125 x 1.125
CNRM-CM6-1	Centre National de Recherches Météorologiques–Centre Européen de Recherche et de Formation Avancée en Calcul Scientifique, France	1.406 x 1.406
INM-CM4-8	Institute for Numerical Mathematics, Russian Academy of Science, Moscow, Russia	1.500 x 2.000
MPI-ESM1-2-LR	Max Planck Institute for Meteorology, Germany	1.875 x 2.500
MRI-ESM2-0	Meteorological Research Institute, Japan	1.125 x 1.125
MIROC6	Japan Agency for Marine-Earth Science and Technology, Atmosphere and Ocean Research Institute, Japan	1.406 x 1.406

For statistical downscaling techniques, we employed the widely used empirical quantile mapping (EQM) method (Eq. 6). EQM calibrates a model's cumulative distribution function (CDF) by adjusting both the mean and individual delta changes for observed climate variable quantiles [8]. It has the advantage of producing adjusted empirical CDFs (ECDFs) for dry and wet days and can simultaneously correct precipitation occurrence frequencies and standard deviations [9]. The EQM method corrects means, variances, quantiles, wet day frequencies, and intensities while nonlinearly preserving extreme values [9]. Therefore, the variability of corrected data is more consistent with the original GCMs data [10].

$$P_{corr}^{EQM} = ECDF_{Obs}^{-1}(ECDF_{GCM}(P_{GCM}) \quad (6)$$

where P_{corr}^{EQM} is the bias corrected precipitation, $ECDF_{Obs}^{-1}$ is the inverse of empirical cumulative distribution function of observed precipitation, $ECDF_{GCM}$ is empirical cumulative distribution function of GCM precipitation, and P_{GCM} is raw precipitation data from the GCMs.

Table S4. Mann–Kendall and Sen's slope results for rainfall (mm/year) and maximum and minimum temperature (°C/year) trends.

Climate variables		Agroecology											
		Wet Wurch			Moist Dega			Moist Weyna Dega			Moist Kolla		
		Observed	SSP2-4.5	SSP5-8.5	Observed	SSP2-4.5	SSP5-8.5	Observed	SSP2-4.5	SSP5-8.5	Observed	SSP2-4.5	SSP5-8.5
Rainfall	z-stat	1.4	2.53*	5.95*	0.86	2.31*	6.01*	1.35	2.81*	5.73*	2.47*	3.11*	5.96*
	Sen's Slope	0.03	1.59	5.91	2.59	1.27	5.07	2.04	1.4	3.97	4.80	1.55	3.55
Maximum temperature	z-stat	4.40*	9.16*	10.26*	4.40*	9.22*	10.32*	2.44*	9.47*	10.31*	1.21	9.47*	10.41*
	Sen's Slope	0.03	0.02	0.03	0.03	0.02	0.03	0.02	0.02	0.03	0.01	0.02	0.03
Minimum temperature	z-stat	5.30*	9.67*	10.35*	5.76*	9.6*	10.41*	4.18*	9.63*	10.49*	4.89*	9.66*	10.5*
	Sen's Slope	0.05	0.02	0.03	0.03	0.02	0.04	0.04	0.03	0.05	0.05	0.03	0.06

* Statistically significant at 5% significant level.

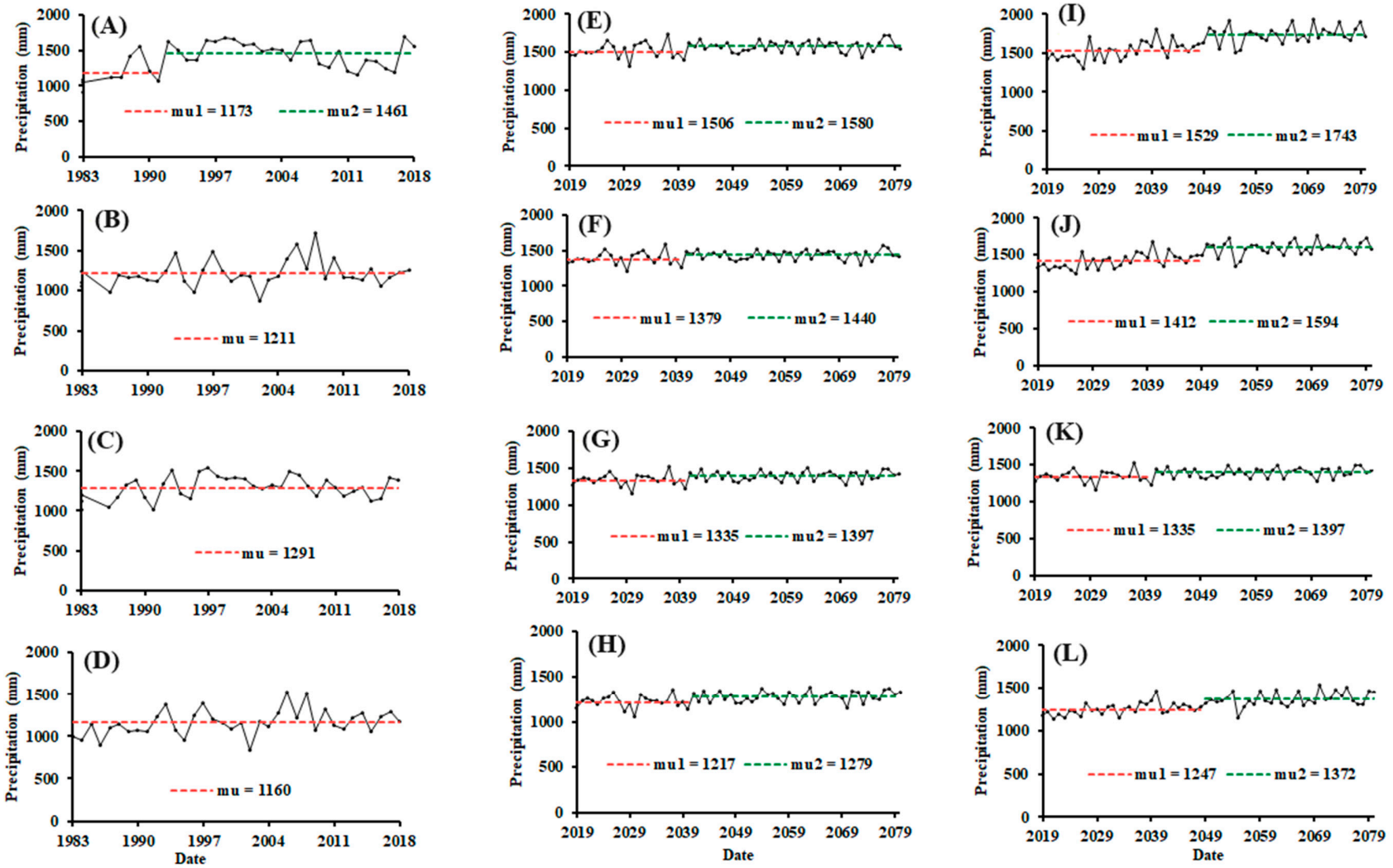

Figure S4. Pettitt's test for change point detection in historical rainfall (A–D) and future downscaled rainfall under the SSP2-4.5 climate scenario (E–H) and under the SSP5-8.5 climate scenario (I–L) in the Wet Wurch, Moist Dega, Moist Weyna Dega, and Moist Kolla agroecological environments, respectively. Where mu1 and mu2 are the mean precipitation before and after change point has occurred respectively.

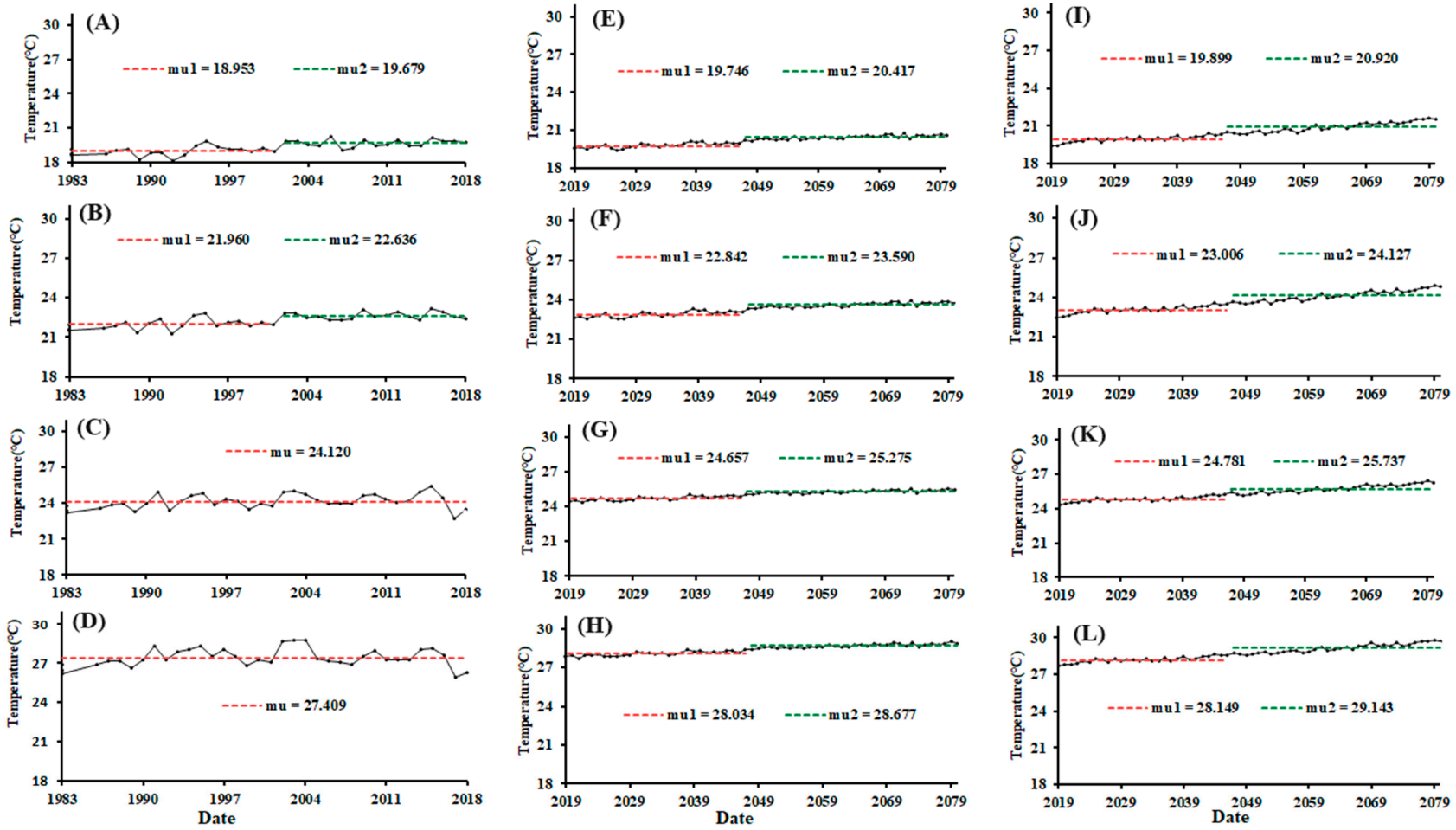

Figure S5. Pettitt's test for change point detection in historical maximum temperature (A–D) and future downscaled maximum temperature under the SSP2-4.5 climate scenario (E–H) and under the SSP5-8.5 climate scenario (I–L) in the Wet Wurch, Moist Dega, Moist Weyna Dega, and Moist Kolla agroecological environments respectively. Where mu1 and mu2 are the mean maximum temperature before and after change point has occurred respectively.

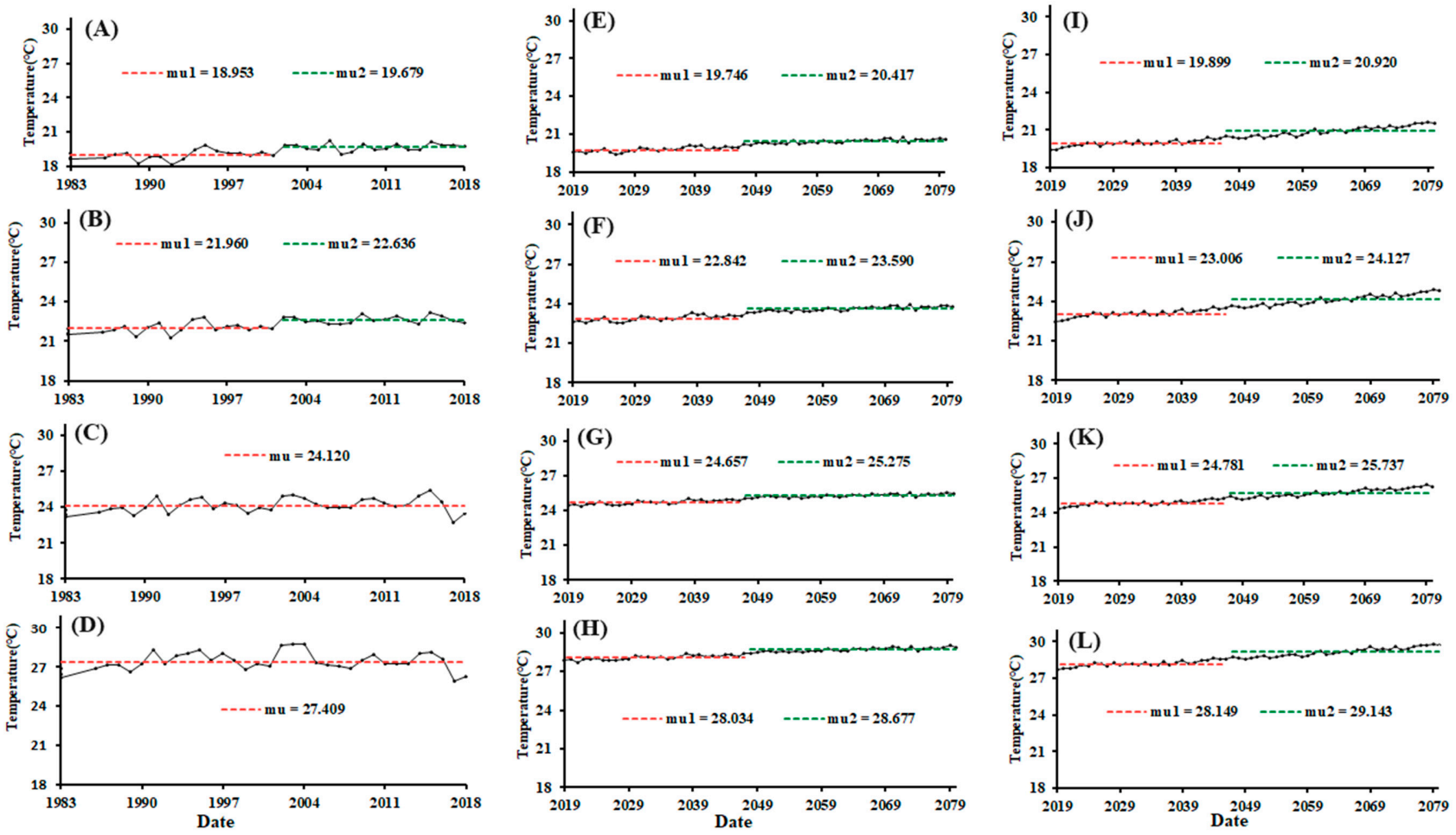

Figure S6. Pettitt's test for change point detection in historical minimum temperature (A–D) and future downscaled minimum temperature under the SSP2-4.5 climate scenario (E–H) and under the SSP5-8.5 climate scenario (I–L) in the Wet Wurch, Moist Dega, Moist Weyna Dega, and Moist Kolla agroecological environments, respectively. Where mu1 and mu2 are the mean minimum temperature before and after change point has occurred respectively.

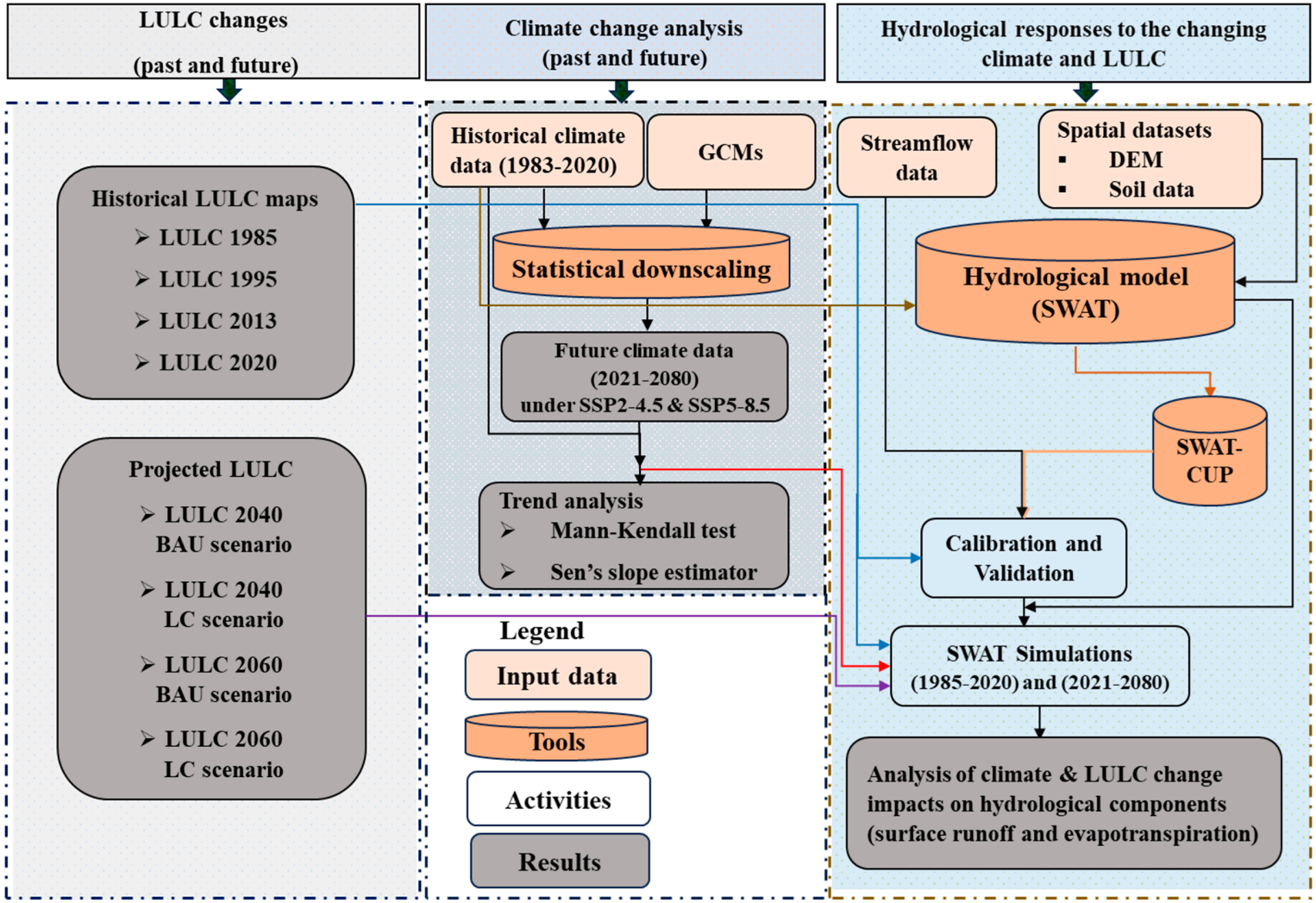

Figure S7. Methodological framework employed for land use/land cover and climate change impact studies on water balance. The land use/land cover (LULC) datasets utilized in this study were obtained from [2]. BAU (business-as-usual) and LC (Land conservation), representing different LULC projection scenarios.

Table S5. SWAT model parameters with their initial values.

Parameter	Description	Initial range
r_CN2.mgt	SCS runoff curve number for moisture condition II	35–98
v_REVAPMN.gw	Threshold depth of water (mm) in the shallow aquifer for 'revap' to occur	0–500
v_GW_REVAP.gw	Groundwater 'revap' coefficient	0.02–0.2
v_GW_DELAY.gw	Groundwater delay (days)	0–500
v_ALPHA_BF.gw	Baseflow alpha factor (days)	0–1
v_GWQMN.gw	Threshold depth of water (mm) in the shallow aquifer required for return flow to occur	0–5000
r_ESCO.hru	Soil evaporation compensation factor	0–1
r_HRU_SLP.hru	Average slope steepness	0–1
r_SLSUBBSN.hru	Average slope length	10–150
r_CH_K2.rte	Effective hydraulic conductivity in main channel alluvium	-0.01–500
r_CH_N2.rte	Manning's 'n' value for the main channel	-0.01–0.3
r_SURLAG.bsn	Surface runoff lag time	0.05–24
r_SOL_BD.sol	Moist bulk density	0–1
r_SOL_AWC.sol	Available water capacity of the soil layer	0–1
r_SOL_K.sol	Saturated hydraulic conductivity	0–2000
r_SOL_CBN.sol	Organic carbon content	0.05–10
r_SOL_ALB.sol	Moist soil albedo	0–0.25
r_SOL_ZMX.sol	Maximum rooting depth of soil profile.	0–3500

Table S6. Final optimized parameter values within the parameter range during the last iteration of calibration.

	Parameter name	Fitted value	Min value	Max value
1	V__REVAPMN.gw	220.17	160.19	289.19
2	V__GW_REVAP.gw	1.73	1.49	2.86
3	R__CH_K2.rte	3.20	-2.86	4.58
4	R__HRU_SLP.hru	-0.20	-0.59	-0.18
5	R__SURLAG.bsn	49.14	48.93	91.57
6	R__CN2.mgt	-0.72	-8.09	2.51
7	V__ALPHA_BF.gw	-13.98	-26.94	-13.23
8	R__SOL_AWC(..).sol	-0.69	-5.98	7.76
9	R__SOL_K(..).sol	29.52	-103.03	201.67
10	V__GW_DELAY.gw	115.80	-148.43	160.61

Note: “R_” refers to a relative change in the parameter where the default values are multiplied by 1 plus a factor in the parameter range, while “V_” refers to the substitution of the default parameter by a value from the parameter range.

2A. Model performance evaluation

During both the calibration and validation phases, the model's performance was assessed using essential goodness-of-fit evaluation criteria, including the coefficient of determination (R2) [11], Nash and Sutcliffe simulation efficiency (NSE) [12], and percent Bias (PBIAS) [13].

Coefficient of determination

The coefficient of determination (R^2) value, varying from 0 to 1, indicates the extent to which the predicted dispersion accounts for the observed dispersion [13]. If the value is zero, there is no correlation, while a value of 1 suggests that the prediction's dispersion matches that of the observations.

$$R^2 = 1 - \frac{\sum(Simulated\ flow - average\ simulated\ flow)^2}{\sum(Observed\ flow - average\ observed\ flow)^2}$$

Nash–Sutcliffe efficiencies

The Nash-Sutcliffe efficiencies (NSE) vary between infinity and one, computed by assessing the model's fitness against the variance of observed data [13]. An NSE value of one indicates an exact alignment between the modeled discharge and the measured data. It is calculated as one minus the total of the absolute squared deviations between predicted and observed values, normalized by the variance of the observed values within the specified investigation period.

$$NSE = 1 - \frac{\sum(Simulated\ flow\ (i) - observed\ flow)^2}{\sum(Observed\ flow\ (i) - average\ observed\ flow)^2}$$

Percent of bias

The percentage of bias (PBIAS) assesses how the simulated values generally lean towards being either larger or smaller than their observed equivalents. An ideal PBIAS value is zero. PBIAS represents the percentage-based variance between the data being assessed. A positive PBIAS value suggests that the model tends to underestimate measured values, while negative values imply an overestimation [13].

$$PBIAS = \sum \frac{Simulated\ flow - observed\ flow}{Observed\ flow} \times 100$$

According to Moriasi [13], model performance is categorized as excellent if R^2 or NSE is equal to or greater than 0.90, very good if it falls within the range of 0.75 to 0.89, good if it ranges from 0.50 to 0.74, fair if it falls between 0.25 to 0.49, poor if it's between 0 and 0.24, and unsatisfactory if R^2 or NSE is less than 0.

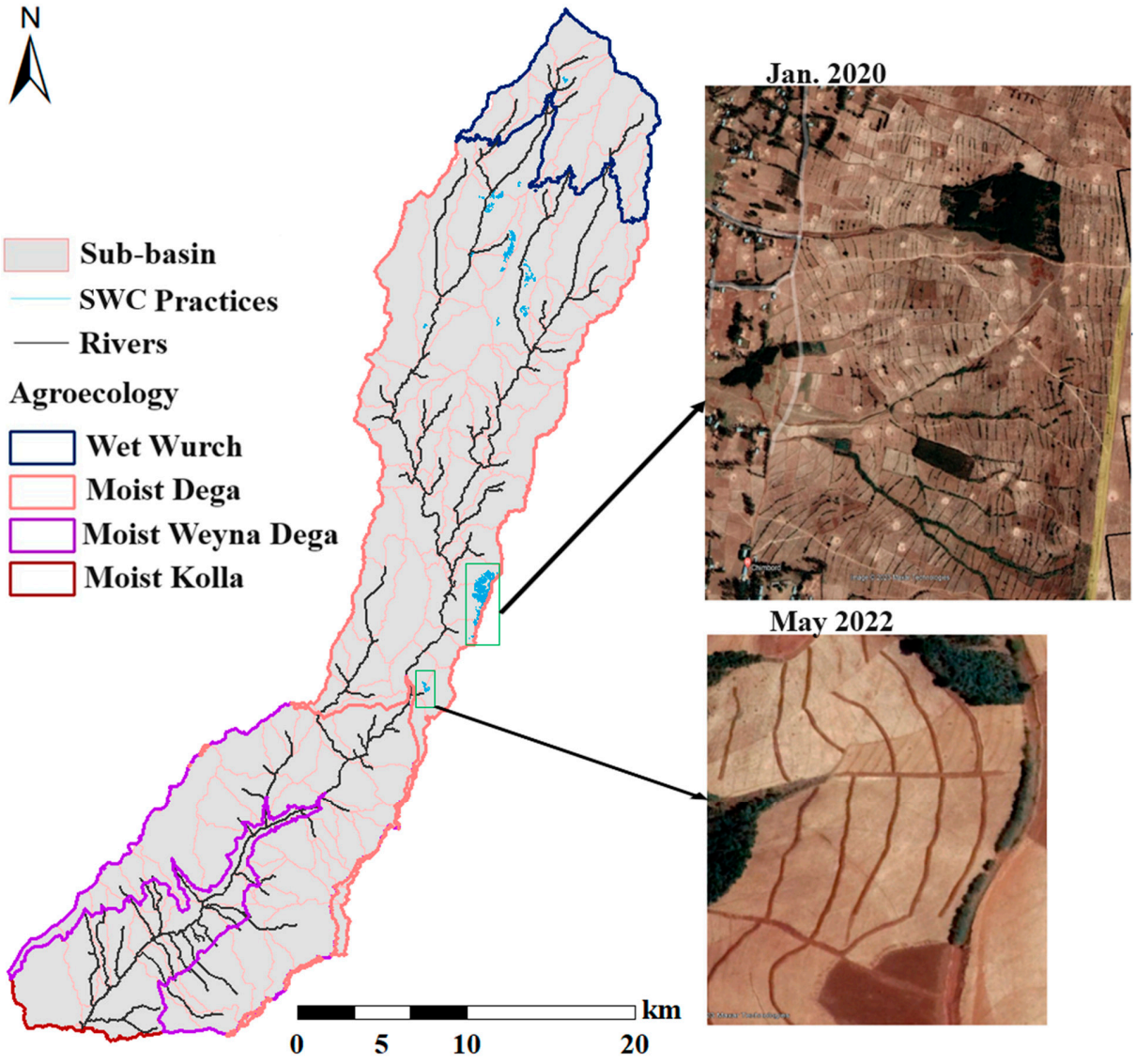

Figure S8. Soil and Water Conservation (SWC) practices (bunds with/out grass) identified, along with the corresponding images captured from Google Earth.

Table S7. The SWAT model simulated results of hydrological responses to the separate and combined impacts of climate and land use/land cover (LULC) changes. RF is the mean annual rainfall, SR is annual runoff, and ET is annual evapotranspiration. The bolded climate periods after 2020 represent the SSP5-8.5 scenario while the non-bolded periods after 2020 represent the SSP2-4.5 climate scenario. * denotes for projected LULC under the LC scenario; values without * are for the BAU scenario projection.

Scenario	LULC	Climate period	RF (mm)	SR (mm)	ET (mm)	Scenario	LULC	Climate period	SR (mm)	SR (mm)	ET (mm)
S1	1985	1983–2002	1232	434	320	S15	2040	**2051–2080**	1458	741	380
S2	1985	2003–2020	1286	430	350	S16	2060	2021–2050	1311	764	351
S3	1995	1983–2002	1232	483	316	S17	2060	**2021–2050**	1352	774	351
S4	1995	2003–2020	1286	484	345	S18	2060	2051–2080	1311	794	370
S5	2013	1983–2002	1232	544	312	S19	2060	**2051–2080**	1458	809	378
S6	2013	2003–2020	1286	563	338	S20	2040*	2003–2020	1286	500	349
S7	2020	1983–2002	1232	615	303	S21	2040*	2021–2050	1311	533	371
S8	2020	2003–2020	1286	626	334	S22	2040*	**2021–2050**	1352	539	376
S9	2040	2003–2020	1286	690	322	S23	2040*	2051–2080	1311	550	390
S10	2020	2021–2050	1311	631	351	S24	2040*	**2051–2080**	1458	557	396
S11	2020	**2021–2050**	1352	639	353	S25	2060*	2021–2050	1311	518	372
S12	2040	2021–2050	1311	698	349	S26	2060*	**2021–2050**	1352	523	376
S13	2040	**2021–2050**	1352	710	353	S27	2060*	2051–2080	1311	528	391
S14	2040	2051–2080	1311	719	367	S28	2060*	**2051–2080**	1458	536	402

Table S8. SWAT model simulated results of hydrological responses to the separate and combined impacts of climate and land use/land cover (LULC) changes in four agroecological environments. RF denotes the mean annual rainfall; SR, the mean annual runoff; and ET, the mean annual evapotranspiration. The bolded climate periods represent the SSP5-8.5 climate scenario while the non-bolded periods represent the SSP2-4.5 climate scenario. * denotes the LULC map for projected LULC under the LC scenario; values without * are for the BAU scenario projection.

Agroecology	Scenario	LULC	Climate period	RF (mm)	SR (mm)	ET (mm)	Scenario	LULC	Climate period	RF (mm)	SR (mm)	ET (mm)
Wet Wurch	S1	1985	1983–2002	1394	309	294	S15	2040	**2051–2080**	1600	637	330
	S2	1985	2003–2020	1423	311	310	S16	2060	2021–2050	1421	654	306
	S3	1995	1983–2002	1394	405	285	S17	2060	**2021–2050**	1465	664	303
	S4	1995	2003–2020	1423	406	310	S18	2060	2051–2080	1419	664	321
	S5	2013	1983–2002	1437	475	282	S19	2060	**2051–2080**	1600	698	322
	S6	2013	2003–2020	1424	483	299	S20	2040*	2003–2020	1423	434	309
	S7	2020	1983–2002	1394	522	277	S21	2040*	2021–2050	1421	438	323
	S8	2020	2003–2020	1423	522	296	S22	2040*	**2021–2050**	1465	441	328
	S9	2040	2003–2020	1423	588	292	S23	2040*	2051–2080	1419	444	340
	S10	2020	2021–2050	1421	523	319	S24	2040*	**2051–2080**	1600	457	353
	S11	2020	**2021–2050**	1465	530	317	S25	2060*	2021–2050	1421	434	330
	S12	2040	2021–2050	1421	593	311	S26	2060*	**2021–2050**	1465	435	340
	S13	2040	**2021–2050**	1465	608	315	S27	2060*	2051–2080	1419	436	351
	S14	2040	2051–2080	1419	605	327	S28	2060*	**2051–2080**	1600	437	357
Moist Dega	S1	1985	1983–2002	1267	559	309	S15	2040	**2051–2080**	1491	751	366
	S2	1985	2003–2020	1284	562	337	S16	2060	2021–2050	1320	757	347
	S3	1995	1983–2002	1267	580	310	S17	2060	**2021–2050**	1372	775	343
	S4	1995	2003–2020	1284	583	335	S18	2060	2051–2080	1314	781	363
	S5	2013	1983–2002	1289	613	304	S19	2060	**2051–2080**	1491	813	369
	S6	2013	2003–2020	1284	630	332	S20	2040*	2003–2020	1284	520	344
	S7	2020	1983–2002	1267	632	299	S21	2040*	2021–2050	1320	545	364
	S8	2020	2003–2020	1284	647	332	S22	2040*	**2021–2050**	1372	557	368
	S9	2040	2003–2020	1284	694	316	S23	2040*	2051–2080	1314	555	379
	S10	2020	2021–2050	1320	635	336	S24	2040*	**2051–2080**	1491	579	384
	S11	2020	**2021–2050**	1372	642	338	S25	2060*	2021–2050	1320	528	363
	S12	2040	2021–2050	1320	694	339	S26	2060*	**2021–2050**	1372	543	363

	S13	2040	**2021–2050**	1372	712	342	S27	2060*	2051–2080	1314	545	392
	S14	2040	2051–2080	1314	715	360	S28	2060*	**2051–2080**	1491	562	398
Moist Weyna	S1	1985	1983–2002	1183	517	302	S15	2040	**2051–2080**	1446	819	399
Dega	S2	1985	2003–2020	1277	522	332	S16	2060	2021–2050	1303	829	358
	S3	1995	1983–2002	1183	573	300	S17	2060	**2021–2050**	1353	842	363
	S4	1995	2003–2020	1277	595	327	S18	2060	2051–2080	1297	857	385
	S5	2013	1983–2002	1192	635	296	S19	2060	**2051–2080**	1446	877	392
	S6	2013	2003–2020	1277	665	325	S20	2040*	2003–2020	1278	533	346
	S7	2020	1983–2002	1183	696	296	S21	2040*	2021–2050	1303	547	382
	S8	2020	2003–2020	1277	714	325	S22	2040*	**2021–2050**	1353	567	392
	S9	2040	2003–2020	1278	774	323	S23	2040*	2051–2080	1299	558	417
	S10	2020	2021–2050	1303	734	364	S24	2040*	**2051–2080**	1445	590	426
	S11	2020	**2021–2050**	1353	748	370	S25	2060*	2021–2050	1303	536	390
	S12	2040	2021–2050	1303	789	359	S26	2060*	**2021–2050**	1353	546	397
	S13	2040	**2021–2050**	1353	795	364	S27	2060*	2051–2080	1299	541	418
	S14	2040	2051–2080	1299	798	389	S28	2060*	**2051–2080**	1446	553	431
Moist Kolla	S1	1985	1983–2002	1119	50	376	S15	2040	**2051–2080**	1471	523	155
	S2	1985	2003–2020	1232	51	409	S16	2060	2021–2050	1244	618	136
	S3	1995	1983–2002	1119	74	359	S17	2060	**2021–2050**	1235	628	139
	S4	1995	2003–2020	1232	105	393	S18	2060	2051–2080	1263	690	150
	S5	2013	1983–2002	1131	270	339	S19	2060	**2051–2080**	1310	648	155
	S6	2013	2003–2020	1232	306	367	S20	2040*	2003–2020	1234	450	115
	S7	2020	1983–2002	1119	406	342	S21	2040*	2021–2050	1244	483	140
	S8	2020	2003–2020	1232	421	370	S22	2040*	**2021–2050**	1235	474	145
	S9	2040	2003–2020	1234	470	113	S23	2040*	2051–2080	1263	494	153
	S10	2020	2021–2050	1243	441	140	S24	2040*	**2051–2080**	1310	490	158
	S11	2020	**2021–2050**	1234	446	145	S25	2060*	2021–2050	1244	464	140
	S12	2040	2021–2050	1244	479	137	S26	2060*	**2021–2050**	1235	441	145
	S13	2040	**2021–2050**	1235	498	143	S27	2060*	2051–2080	1263	484	154
	S14	2040	2051–2080	1263	501	152	S28	2060*	**2051–2080**	1310	481	160

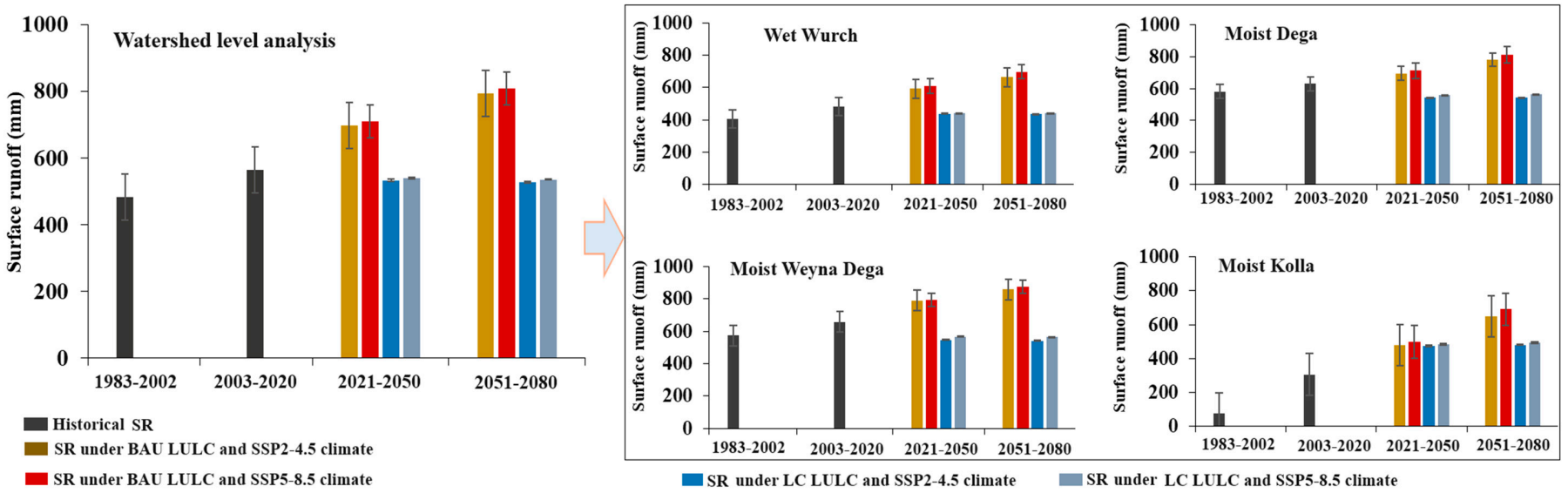

Figure S9. Mean annual surface runoff (SR) both at the watershed level (on the left) and across four distinct agroecological environments (on the right). BAU (business-as-usual) and LC (Land conservation), representing different LULC projection scenarios. The error bars represent the temporal dynamics of evapotranspiration and overlapping bars imply no significant difference between adjacent time periods.

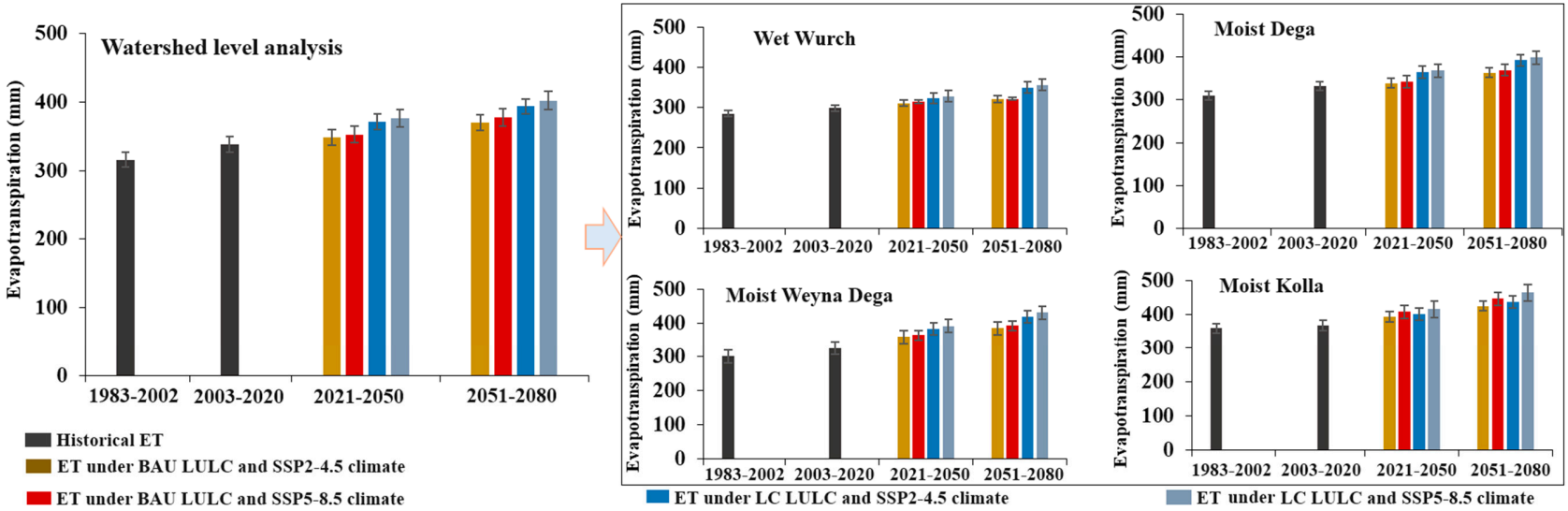

Figure S10. Mean annual Evapotranspiration (ET) both at the watershed level (on the left) and across four distinct agroecological environments (on the right). BAU (business-as-usual) and LC (Land conservation), representing different LULC projection scenarios. The error bars represent the temporal dynamics of evapotranspiration and overlapping bars imply no significant difference between adjacent time periods.

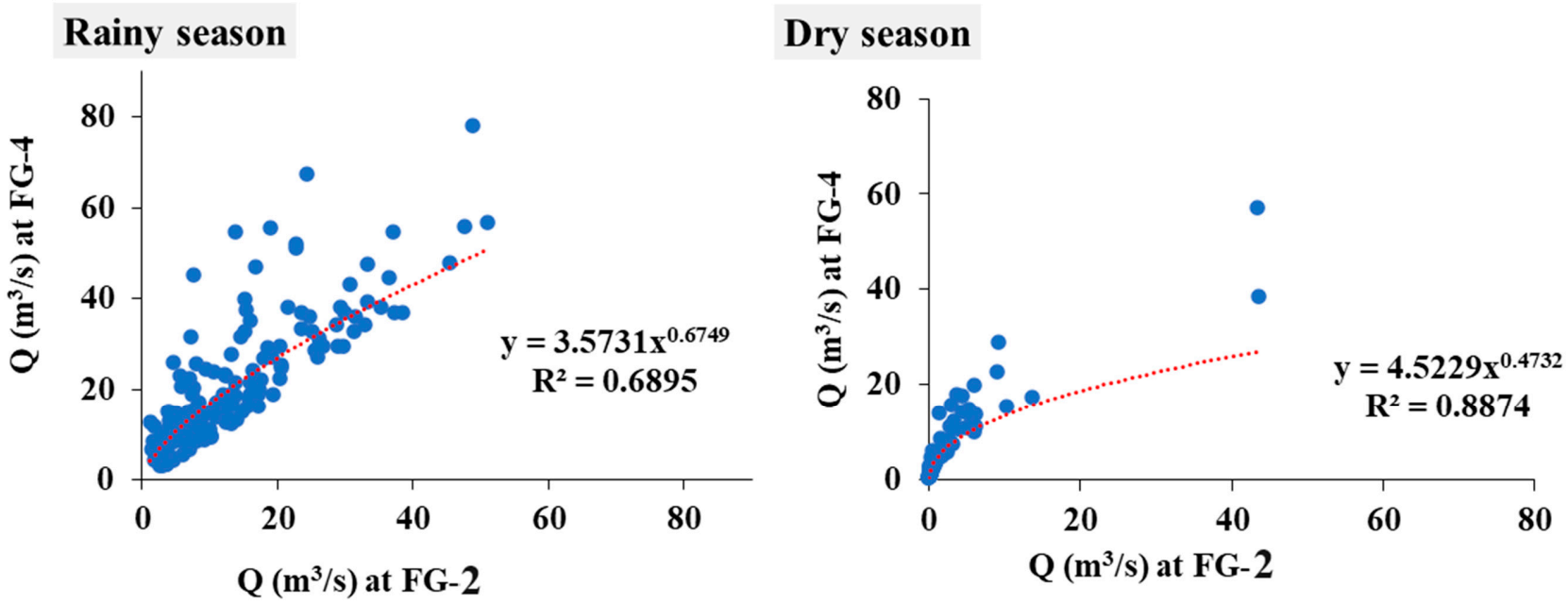

Figure S11. Correlation of streamflow between stations FG-2 and FG-4 in the rainy and dry seasons.

References

1. Boori, M. S.; Paringer, R.; Choudhary, K.; Kupriyanov, A. Supervised and unsupervised classification for obtaining land use/cover classes from hyperspectral and multi-spectral imagery. In *Sixth International Conference on Remote Sensing and Geoinformation of the Environment (RSCy2018)*; SPIE, 2018; Vol. 10773, pp 191–201.

2. Meshesha, T. M.; Tsunekawa, A.; Haregeweyn, N.; Tsubo, M.; Fenta, A. A.; Berihun, M. L.; et al. Agroecology-based land use/land cover change detection, prediction, and its implications for land degradation: a case study in the Upper Blue Nile Basin. *International Soil and Water Conservation Research* **2024**, *12*(1), 1–12.

3. Eastman, J. R. TerrSet 2020–Geospatial Monitoring and Modeling System Manual. *Worcester, MA: Clark Labs, Clark University* **2020**.

4. Bunyangha, J.; Majaliwa, M. J. G.; Muthumbi, A. W.; Gichuki, N. N.; Egeru, A. Past and future land use/land cover changes from multi-temporal Landsat imagery in Mpologoma catchment, eastern Uganda. *Egyptian Journal of Remote Sensing and Space Science* **2021**, *24*(3), 675–685. doi: 10.1016/j.ejrs.2021.02.003.

5. Berihun, M. L.; Tsunekawa, A.; Haregeweyn, N.; Tsubo, M.; Fenta, A. A.; Ebabu, K.; et al. Reduced runoff and sediment loss under alternative land capability-based land use and management options in a sub-humid watershed of Ethiopia. *Journal of Hydrology: Regional Studies* **2022**, *40*, 100998.

6. Kindu, M.; Schneider, T.; Döllerer, M.; Teketay, D.; Knoke, T. Scenario modelling of land use/land cover changes in Munessa-Shashemene landscape of the Ethiopian highlands. *Science of the Total Environment* **2018**, *622–623*, 534–546. doi: 10.1016/j.scitotenv.2017.11.338.

7. Jagger, P. A. management of less-favored lands: Policies for sustainable land management in the highlands of Ethiopia. **2015**, No. August 22–23.

8. Holthuijzen, M.; Beckage, B.; Clemins, P. J.; Higdon, D.; Winter, J. M. Robust bias-correction of precipitation extremes using a novel hybrid empirical quantile-mapping method: Advantages of a linear correction for extremes. *Theoretical and Applied Climatology* **2022**, *149*(1–2), 863–882.

9. Enayati, M.; Bozorg-Haddad, O.; Bazrafshan, J.; Hejabi, S.; Chu, X. Bias correction capabilities of quantile mapping methods for rainfall and temperature variables. *Journal of Water and Climate Change* **2021**, *12*(2), 401–419.

10. Cannon, A. J.; Sobie, S. R.; Murdock, T. Q. Bias correction of GCM precipitation by quantile mapping: how well do methods preserve changes in quantiles and extremes? *Journal of Climate* **2015**, *28*(17), 6938–6959.

11. Krause, P.; Boyle, D. P.; Bäse, F. Comparison of different efficiency criteria for hydrological model assessment. *Advances in geosciences* **2005**, *5*, 89–97.

12. Nash, J. E.; Sutcliffe, J. V. River flow forecasting through conceptual models' part I—A discussion of principles. *Journal of hydrology* **1970**, *10*(3), 282–290.

13. Moriasi, D. N.; Arnold, J. G.; Van Liew, M. W.; Bingner, R. L.; Harmel, R. D.; Veith, T. L. Model evaluation guidelines for systematic quantification of accuracy in watershed simulations. *Transactions of the ASABE* **2007**, *50*(3), 885–900.